V.G. Pol, J.M. Calderon-Moreno and M.M. Thackeray

A photoactive titanate with a stereochemically active Sn lone pair: Electronic and crystal structure of Sn_2TiO_4 from computational chemistry

Lee A. Burton, Aron Walsh*

Centre for Sustainable Chemical Technologies and Department of Chemistry, University of Bath, UK

ABSTRACT

TiO_2 remains the most widely studied metal oxide for photocatalytic reactions. The standard approach to reduce the band gap of titania, for increasing the absorption of visible light, is anion modification. For example the formation of an oxynitride compound, where the nitrogen 2p states decrease the binding energy of the valence band. We demonstrate that cation modification can produce a similar effect through the formation of a ternary oxide combining Ti and an ns^2 cation, Sn(II). In Sn_2TiO_4, the underlying Ti 3d conduction states remain largely unmodified and an electronic band gap of 2.1 eV (590 nm) is predicted by hybrid density functional theory. Our analysis indicates a strong potential for Sn_2TiO_4 in visible-light driven photocatalysis, which should prove superior to the alternative $(SnO_2)_{1-x}(TiO_2)_x$ solid-solution.

© 2012 Elsevier Inc. All rights reserved.

1. Introduction

Metal oxides are widely studied for solar harvesting applications, despite the fact that the majority of metal oxides have optical band gaps that transmit a large fraction of the terrestrial solar spectrum. Indeed, while the most studied material titanium dioxide (TiO_2) is catalytically active for the water-splitting reaction [1], the theoretical maximum solar-to-H_2 conversion efficiency is only of the order of 1%, given its large optical band gap of ca. 3.2 eV [2]. One major challenge in the field of energy materials is to design, or discover, new metal oxide systems that can absorb significant fractions of visible light in order to make commercial devices economically viable in a competitive market place [3–5].

TiO_2 has been studied for applications ranging from heterogeneous catalysis to dye sensitized solar cells [6–8]. Despite its large optical band gap, partially reduced TiO_2 conducts electrons, i.e., $TiO_{2-\delta}$ is an n-type wide band gap semiconductor. Ti(IV) has a valence electronic configuration of $3d^0$, with the unoccupied 3d states forming the conduction band. In the presence of excess electrons, paramagnetic Ti(III) $3d^1$ species can also be formed, and in significant concentrations they can change the color of the material from white to black, with the limiting compound Ti_2O_3 being a Mott-insulator [9]. The defect chemistry and physics of TiO_2 has resulted in a substantial amount of literature in recent years [10–18]. The most promising progress towards obtaining a higher-efficiency TiO_2 based photocatalyst has involved: (i) the

incorporation of nitrogen [19]; (ii) co-doping of multiple anions [20]; (iii) the application of epitaxial or uniaxial strain [21]. An alternative approach is to introduce post-transition metal oxides with filled low binding energy s states.

In comparison to TiO_2, stannous oxide (SnO) features a smaller and indirect band gap (0.7–1.3 eV), and has been the subject of recent attention owing to its hole mediated electrical conductivity (p-type conduction) [22]. Sn(II) has an occupied $5s^2$ state around 7 eV below the top of the valence band, which hybridizes with O 2p, and nominally empty Sn 5p states, to produce a local distortion in the Sn electron distribution and coordination environment, resulting in the layered litharge structure [23–25]. The oxide of tetravalent tin (SnO_2) adopts the rutile crystal structure, similar to TiO_2, and exhibits a wider band gap (3.6 eV) as well as electron mediated conductivity (n-type conduction) [26,27].

The combination of Sn(II) and Ti(IV) cations in a single material could be desirable for numerous reasons including the potential for the coexistence of p-type and n-type conductivity for oxide-based electronic applications (e.g., oxide p–n homo-junctions), and a relatively low optical band gap for photocatalysis. Unfortunately, attempts to grow the ternary Sn/Ti oxide system have resulted in anatase or rutile solid solutions containing the Sn(IV) species [28–30], without the presence of the occupied Sn $5s^2$ orbitals. However, Kumada et al. reported the successful synthesis of Sn_2TiO_4 single crystals from TiO_2 and $SnCl_2$ precursors [31], with a more recent report of microwave assisted synthesis by Ohara et al. [32]. The electrical or optical properties of Sn_2TiO_4 have not yet been reported to our knowledge.

In this paper, we report a study of the structural and electronic properties of tin titanate, using an electronic structure approach

* Corresponding author.
E-mail address: a.walsh@bath.ac.uk (A. Walsh).

based on Density Functional Theory (DFT). Preliminary results were reported as part of a perspective on the computational study of energy materials [33], but this work has been extended to include thermodynamic and vibrational properties, in addition to the electronic band structure and alignments. The results compare well to the limited experimental data available to date, including the recently measured vibrational spectrum. We call for further studies on the topic in order to verify our predictions in relation to the electronic and optical properties of the material, and to assess its photocatalytic activity.

2. Computational methodology

Total energy electronic structure calculations were performed within the framework of DFT [34,35], using periodic boundary conditions to represent the perfect solid [36]. The all-electron FHI-AIMS code [37,38] was employed, which constructs the electronic wavefunction using a basis set composed of numeric atom-centered orbitals. In this study, a "Tier-2" basis set was employed with a $6 \times 6 \times 8$ special k-point grid, and scalar-relativistic effects treated at the scaled ZORA level [39]. Relativistic corrections were found to be important in the correct description of the Sn 5s band energy, which for an atomic calculation increases the binding energy by 0.75 eV. Exchange–correlation effects were described through the generalized gradient approximation, with the semi-local Perdew–Burke–Ernzerhof functional revised for solids (PBEsol) [40].

In order to obtain a more quantitative band gap prediction, hybrid-DFT calculations were also performed in which 25% of the short-range semi-local exchange functional was replaced with exact non-local Hartree–Fock exchange, and screening ($\omega = 0.11$ Bohr^{-1}) was applied to partition the Coulomb potential in short-range (SR) and long-range (LR) components: the HSE06 functional [41–43]. This functional is known to perform well for the parent compound TiO$_2$ [44]. All hybrid functional calculations [45,46] were performed in the code VASP [47,48]. For these calculations, equivalent k-point meshes were combined with a well-converged 500 eV plane-wave cutoff for the basis set. For the same choice of density functional, comparable results were obtained with both VASP and FHI-AIMS.

3. Crystal structure

The crystal structure for Sn$_2$TiO$_4$ determined by Kumada et al. [31] is isostructural to "red lead" (Pb$_3$O$_4$) as shown in Fig. 1. Pb$_3$O$_4$ has a crystal structure (space group P4$_2$/mbc, D$_{4h}^{13}$) containing two distinct cation sites characteristic of the Pb atoms found in both litharge Pb(II)O (8h Wyckoff position, pyramidal arrangement with three nearest-neighbor oxygens) and rutile Pb(IV)O$_2$ (4d Wyckoff position, distorted oxygen octahedron), respectfully [49]. Despite
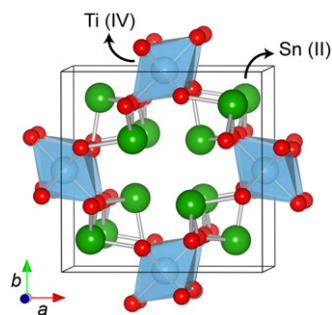
being considered of the mineral spinel class, its crystal structure is unique and occurs only for a handful of other materials including Sb$_2$CoO$_4$, Pb$_2$SnO$_4$ and Sb$_2$ZnO$_4$ [50]. There are 28 atoms per crystallographic unit cell and a notable hollow in the center of the crystal, understood to be stabilized by van der Waals interactions between the lone pair electrons [51]. The synthesis of Sn$_2$TiO$_4$ in the Pb$_3$O$_4$ structure is therefore not unexpected given that it simultaneously satisfies the coordination preferences of both the Ti(IV) and Sn(II) ions.

Taking the reported crystal structure as a starting point, both the internal positions and lattice vectors were optimized to their equilibrium positions for each density functional under the constraint of tetragonal symmetry. The equilibrium structural parameters are collected in Table 1. The calculated lattice constants are within 1% of experiment and the local bonding environments are well reproduced, namely, the mildly distorted Ti octahedra and the highly distorted four coordinate Sn site.

The vibrational spectra of Sn$_2$TiO$_4$ single crystals have been recently measured [52], with a small number of sharp peaks observed in the Raman spectrum. While there exists 84 vibrational modes, owing to the 28 atoms in the unit cell, these are significantly reduced by the symmetry selection rules. Analysis of the calculated phonon frequencies, under point group D$_{4h}$, results in a set of four Raman active peaks from 250 to 300 cm^{-1} (B$_{2g}$, A$_{1g}$ and E$_g$), an isolated peak at 475 cm^{-1} (A$_{1g}$), and the highest intensity peak present at 628 cm^{-1} (A$_{1g}$). These are in excellent agreement with the reported spectrum [52].

4. Thermodynamic properties

Given the absence of available experimental data, we have calculated the fundamental thermodynamic properties of Sn$_2$TiO$_4$, which will be of importance for the design of efficient synthetic routes, as well as the control of phase equilibria. The enthalpy of formation,

$$(\Delta H_f)\ 2Sn(s) + Ti(s) + 2O_2(g) \rightarrow Sn_2TiO_4$$
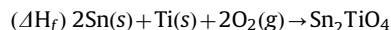
is found to be -1406.8 kJ/mol, indicative that the isolated stoichiometric compound is stable thermodynamically. The enthalpy of mixing with respect to the parent binary oxides
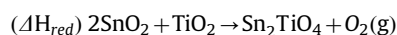
$$(\Delta H_{mix})\ 2SnO + TiO_2 \rightarrow Sn_2TiO_4$$
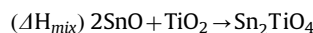
is -0.5 kJ/mol, which is consistent with the slow reaction rate for solid-state synthesis that can be substantially promoted by microwave irradiation [32]. Finally, the probability for formation of the ternary material from a mixture of rutile dioxides can be assessed

Fig. 1. The crystal structure of Sn$_2$TiO$_4$. The Ti distorted octahedral are filled blue; Sn atoms are colored green, and oxygen coloured red.

Table 1
Equilibrium structural paramaters of Sn$_2$TiO$_4$ derived from experiment [31] and computation (PBEsol). The percentage deviations are shown in parenthesis.

	Experiment [31]	PBEsol
a (Å)	8.492	8.474 (-0.21%)
c (Å)	5.923	5.914 (-0.15%)
Volume (Å^3)	426.93	424.68
Ti (4d site)	0, 1/2, 1/4	0, 1/2, 1/4
Sn (8h site)	0.145, 0.163, 0	0.146, 0.161, 0
O (8g site)	0.664, 0.164, 1/4	0.663, 0.164, 1/4
O (8h site)	0.098, 0.621, 0	0.097, 0.621, 0
Sn–O (Å)	2×2.09	2×2.10
	1×2.21	1×2.21
	1×2.76	1×2.77
Ti–O (Å)	2×1.97	2×1.96
	4×1.99	4×1.98

from the reduction reaction:

$$(\Delta H_{red})\ 2SnO_2 + TiO_2 \rightarrow Sn_2TiO_4 + O_2(g)$$

which is calculated to be 480 kJ/mol, which indicates that the spontaneous reduction of Sn(IV) to Sn(II) with the loss of oxygen will not readily occur.

As part of a large-scale search over a wide section of ternary oxide phase space [53], the alternative Sn(II)/Ti(IV) ratio of $SnTiO_3$ was predicted to favour the ilmenite crystal structure. This ABO_3 stoichiometry is also thermodynamically stable, with a calculated formation enthalpy of -1154 kJ/mol. However, there is no driving force for disproportionation: the reaction enthalpy for the conversion of $SnTiO_3$ to Sn_2TiO_4 with the formation of excess TiO_2 is only 4 kJ/mol,

$$(\Delta H_{dis})\ 2SnTiO_3 \rightarrow Sn_2TiO_4 + TiO_2.$$
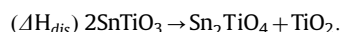
5. Electronic structure

The calculated electronic density of states and electronic band structure are shown in Fig. 2. While the valence band is dominated by O 2p states, the presence of Sn 5s is noted at -7 eV, and to a lesser extent at the top of the valence band. Mixing of Sn 5p is also significant and results in the projected "lone pair" density shown in Fig. 3. These features are consistent with those of SnO [23] and have been reviewed in detail as part of the revised lone pair model [54,55]. Contributions from Ti dominate the conduction band due to the unoccupied low binding energy Ti 3d states, with a similar topology to rutile TiO_2, owing to the common networks of edge sharing Ti–O octahedra. Low energy optical excitations across the band gap of the material will therefore involve excitations from Sn to Ti, which may result in the partial oxidation and reduction of Sn (from oxidation state II to IV) and Ti (from IV to III), respectively. The photochemistry of the material will be addressed in future studies as it involves the application of higher-level computational techniques.

The band structure exhibits a high degree of dispersion at the top of the valence band. The highest occupied states at the gamma and X points are doubly degenerate and composed of Sn s and O p wavefunction character. This can be observed in the band decomposed electron density in Fig. 3, which demonstrates that these states are dominated by a hybridized mixture of Sn s, p and O p atomic orbitals. The density node between Sn and O is indicative of the antibonding nature of this interaction at the top of the valence band, which has been confirmed for SnO [23,25] by crystal orbital overlap population analysis [57]. As the difference between the valence band maxima at Γ and X is less than 5 meV, it is uncertain whether the fundamental electronic band gap is formally direct or indirect. Nonetheless, the difference between
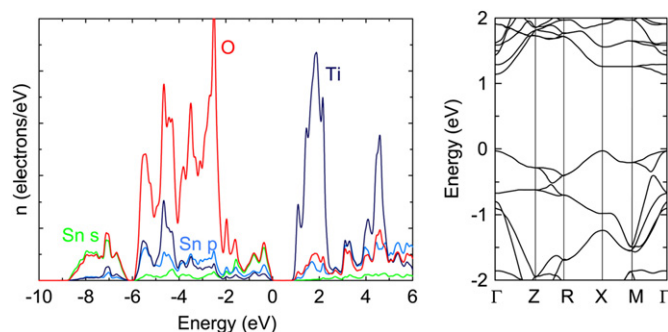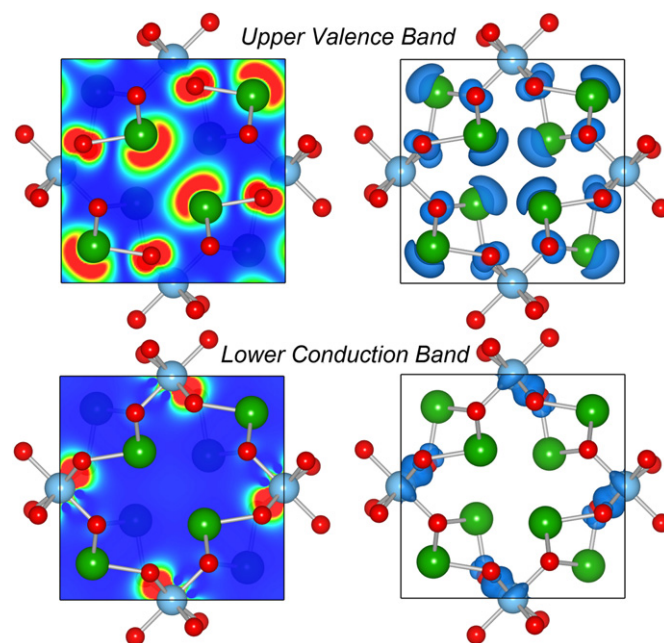

Fig. 3. Calculated electron density contour maps (left) and 3D isosurface (right) associated the upper valence band and lower conduction band of Sn_2TiO_4. Contour maps are plotted from blue (zero density) to red (high density) using the VESTA [58] software package. (For interpretation of the references to color in this figure legend, the reader is reffered to the web version of this article.)

the two is small so that a strong onset of optical absorption is expected. The location of the conduction band minimum is unambiguous, being centered at the Γ point, and composed of predominately Ti d character.

While the PBEsol functional can provide accurate predictions of the structural and thermodynamic properties of materials, the electronic band gaps (E_g) of insulators are commonly underestimated significantly. At this level of theory (Fig. 2), the calculated band gap is 1.2 eV, while a more accurate prediction using the hybrid HSE06 functional is 2.1 eV (590 nm). Due to absorption in the green and blue ranges of the spectrum, the ideal material should be red in color and well suited for applications involving the conversion of visible light.

Further to the value of the band gap itself, which is the energy *difference* between the valence and conduction band extrema, the *absolute* band edge positions are of crucial importance for the application of materials in electrical or electrochemical systems [59]. While a robust theory of valence band alignments has been developed for treating tetrahedral semiconductors [60], oxides represent a more challenging case. To this end, we follow the standard empirical approach based on the geometric mean of the Mulliken electronegativity (χ) for the component atoms that was applied by Bulter and Ginley [61] to a range of oxides, and later by Xu and Schoonen [62] to other semiconducting materials. In both studies, reasonable agreement was found with respect to direct electrochemical measurements of the flat band voltage. Here the electron affinity (EA) is defined as:

$$EA = \chi^{mean} - \tfrac{1}{2}E_g.$$

The resulting band energies of Sn_2TiO_4 are plotted in Fig. 4 alongside those of SnO_2 and TiO_2. The smaller band gap of the ternary compound is as a result of the lower binding energy of the valence band, which follows our analysis concerning the crucial role of Sn 5s. The difference in conduction band energies is much smaller, and they decrease monotonically from TiO_2 to SnO_2 to Sn_2TiO_4. While this analysis provides a good qualitative description of the relative electron energies, it should be remembered that

Fig. 2. Calculated electronic density of states and band structure of Sn_2TiO_4. The highest occupied state is set to 0 eV, and the high symmetry points of the first Brillouin zone are taken from Ref [56].
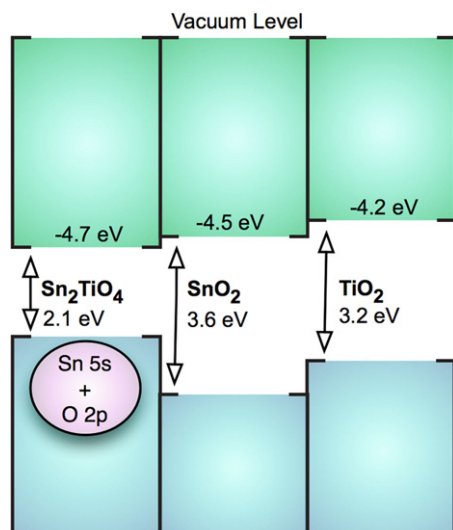
Fig. 4. Predicted electron affinity of Sn_2TiO_4 with respect to the vacuum level, and in comparison to SnO_2 and TiO_2.

effective electron chemical potentials, of interest for electrochemical applications, are intimately dependent on the surface structure and composition (e.g., the presence of a dipole) and surface carrier concentrations.

6. Conclusion

The structural and electronic properties of Sn_2TiO_4 in the Pb_3O_4 structure have been reported from first-principles calculations. The equilibrium crystal structure parameters are found to be in very good agreement with recent X-ray diffraction data. Covalent interactions between O and Sn (Ti) are found to dominate the valence (conduction) band edge. The predicted band gap of 2.1 eV is remarkably small for a Ti containing oxide, but of a similar order to those reported for other ns^2/nd^{10} ternary oxides such as $BiVO_4$. While low band gaps can be found for oxides containing transition metal cations, the polaron-dominated conductivity severely limits optoelectronic and photocatalytic applications. Dispersion in both the valence and conduction band edges is relatively large, indicating the potential for electron and hole conductivity; however, it is unclear whether this material will be intrinsically n-type (as TiO_2) or p-type as (SnO), or whether the low band gap will result in high photocatalytic activity under visible light. These issues should be addressed in future experimental and theoretical studies.

Acknowledgments

References

[1] A. Fujishima, K. Honda, Nature 238 (1972) 37.
[2] T. Bak, J. Nowotny, M. Rekas, C.C. Sorrell, Int. J. Hydrogen Energy 27 (2002) 991.
[3] A. Kudo, Y. Miseki, Chem. Soc. Rev. 38 (2009) 253.
[4] F.E. Osterloh, Chem. Mater. 20 (2008) 35–54.
[5] B.D. Alexander, P.J. Kulesza, I. Rutkowska, R. Solarska, J. Augustynski, J. Mater. Chem. 18 (2008) 2298.
[6] M. Gratzel, Nature 414 (2001) 338–344.
[7] M. Gratzel, Prog. Photovoltaics 8 (2000) 171.
[8] A.L. Linsebigler, G. Lu, J.T. Yates, Chem. Rev. 95 (1995) 735.
[9] N.F. Mott, L. Friedman, Philos. Mag. 30 (1974) 389–402.
[10] B.J. Morgan, D.O. Scanlon, G.W. Watson, J. Mater. Chem. 19 (2009) 5175–5178.
[11] B.J. Morgan, G.W. Watson, Phys. Rev. B 80 (2009) 233102.
[12] B.J. Morgan, G.W. Watson, Surf. Sci. 601 (2007) 5034.
[13] S. Na-Phattalung, M.F. Smith, K. Kim, M.H. Du, S.H. Wei, S.B. Zhang, S. Limpijumnong, Phys. Rev. B 73 (2006).
[14] C.L. Olson, J. Nelson, M.S. Islam, J. Phys. Chem. B 110 (2006) 9995.
[15] C. Di Valentin, G. Pacchioni, A. Selloni, Phys. Rev. Lett. 97 (2006) 166803.
[16] D.C. Sayle, C.R.A. Catlow, M.A. Perrin, P. Nortier, J. Phys. Chem. Solids 56 (1995) 799–805.
[17] C.R.A. Catlow, R. James, W.C. Mackrodt, R.F. Stewart, Phys. Rev. B 25 (1982) 1006.
[18] A. Walsh, C.R.A. Catlow, Chem. Phys. Chem. 11 (2010) 2341–2344.
[19] C. Di Valentin, E. Finazzi, G. Pacchioni, A. Selloni, S. Livraghi, M.C. Paganini, E. Giamello, Chem. Phys. 339 (2007) 44–56.
[20] Y. Gai, J. Li, S.-S. Li, J.-B. Xia, S.-H. Wei, Phys. Rev. Lett. 102 (2009) 036402–036404.
[21] W.-J. Yin, S. Chen, J.-H. Yang, X.-G. Gong, Y. Yan, S.-H. Wei, Appl. Phys. Lett. 96 (2010) 221901–221903.
[22] Y. Ogo, H. Hiramatsu, K. Nomura, H. Yanagi, T. Kamiya, M. Hirano, H. Hosono, Appl. Phys. Lett. 93 (2008) 032113.
[23] A. Walsh, G.W. Watson, Phys. Rev. B 70 (2004) 235114.
[24] G.W. Watson, J. Chem. Phys. 114 (2001) 758–763.
[25] A. Walsh, G.W. Watson, J. Phys. Chem. B 109 (2005) 18868–18875.
[26] J. Robertson, Phys. Rev. B 30 (1984) 3520.
[27] K.G. Godinho, A. Walsh, G.W. Watson, J. Phys. Chem. C 113 (2009) 439.
[28] H. Yamane, B.C. Young, T. Hirai, J. Ceram. Soc. Jpn. 100 (1992) 1473.
[29] T. Hirata, J. Am. Ceram. Soc. 83 (2000) 3205.
[30] M.H. Harunsani, F.E. Oropeza, R.G. Palgrave, R.G. Egdell, Chem. Mater. 22 (2010) 1551–1558.
[31] N. Kumada, Y. Yonesaki, T. Takei, N. Kinomura, S. Wada, Mater. Res. Bull. 44 (2009) 1298.
[32] S. Ohara, H. Takizawa, Y. Hayashi, Chem. Lett. 39 (2010) 364–365.
[33] C.R.A. Catlow, Z.X. Guo, M. Miskufova, S.A. Shevlin, A.G.H. Smith, A.A. Sokol, A. Walsh, D.J. Wilson, S.M. Woodley, Philos. Trans. R. Soc. London, Ser. A 368 (2010) 3379–3456.
[34] P. Hohenberg, W. Kohn, Phys. Rev. 136 (1964) B864.
[35] W. Kohn, L.J. Sham, Phys. Rev. 140 (1965) A1133.
[36] M.C. Payne, M.P. Teter, D.C. Allan, T.A. Arias, J.D. Joannopoulos, Rev. Mod. Phys. 64 (1992) 1045.
[37] V. Havu, V. Blum, P. Havu, M. Scheffler, J. Comput. Phys. 228 (2009) 8367–8379.
[38] V. Blum, R. Gehrke, F. Hanke, P. Havu, V. Havu, X. Ren, K. Reuter, M. Scheffler, Comput. Phys. Commun. 180 (2009) 2175–2196.
[39] E. Vanlenthe, E.J. Baerends, J.G. Snijders, J. Chem. Phys. 101 (1994) 9783–9792.
[40] J.P. Perdew, A. Ruzsinszky, G.I. Csonka, O.A. Vydrov, G.E. Scuseria, L.A. Constantin, X. Zhou, K. Burke, Phys. Rev. Lett. 100 (2008) 136406–136414.
[41] J. Heyd, G.E. Scuseria, M. Ernzerhof, J. Chem. Phys. 118 (2003) 8207–8215.
[42] J. Heyd, G.E. Scuseria, J. Chem. Phys. 121 (2004) 1187–1192.
[43] A.V. Krukau, O.A. Vydrov, A.F. Izmaylov, G.E. Scuseria, J. Chem. Phys. 125 (2006) 224106–224115.
[44] P. Deak, B. Aradi, T. Frauenheim, Phys. Rev. B 83 (2011) 155207.
[45] J. Paier, M. Marsman, K. Hummer, G. Kresse, I.C. Gerber, J.G. Angyan, J. Chem. Phys. 124 (2006) 154709.
[46] M. Marsman, J. Paier, A. Stroppa, G. Kresse, J. Phys. Condens. Matter 20 (2008) 064201.
[47] G. Kresse, J. Furthmüller, Comput. Mater. Sci. 6 (1996) 15.
[48] G. Kresse, J. Furthmüller, Phys. Rev. B 54 (1996) 11169.
[49] A.F. Wells, Structural Inorganic Chemistry, 5th ed., Oxford University Press, Oxford, 1984.
[50] R.W.G. Wyckoff, Crystal Structures, Interscience, New York, 1948 2.
[51] B. Dickens, J. Inorg. Nucl. Chem. 27 (1965) 1509.
[52] E.J. Baran, A.C. Gonzalez-Baro, N. Kumada, N. Kinomura, T. Takei, Y. Yonesaki, J. Alloys Compd. 490 (2010) L12–L14.
[53] G. Hautier, C.C. Fischer, A. Jain, T. Mueller, G. Ceder, Chem. Mater. 22 (2010) 3762–3767.
[54] A. Walsh, D.J. Payne, R.G. Egdell, G.W. Watson, Chem. Soc. Rev. 40 (2011) 4455–4463.
[55] D.J. Payne, R.G. Egdell, A. Walsh, G.W. Watson, J. Guo, P.A. Glans, T. Learmonth, K.E. Smith, Phys. Rev. Lett. 96 (2006) 157403.
[56] M.I. Aroyo, A. Kirov, C. Capillas, J.M. Perez-Mato, H. Wondratschek, Acta Crystallogr., Sect. A 62 (2006) 115.
[57] R. Hoffmann, Angew. Chem. Int. Ed. 26 (1987) 846.
[58] K. Momma, F. Izumi, J. Appl. Crystallogr. 41 (2008) 653.
[59] N.F. Mott, R.W. Gurney, Electronic Processes in Ionic Crystals, Oxford University Press, Oxford, 1940.
[60] Y.-H. Li, A. Walsh, S. Chen, W.-J. Yin, J.-H. Yang, J. Li, J.L.F. Da Silva, X.G. Gong, S.-H. Wei, Appl. Phys. Lett. 94 (2009) 212109–212113.
[61] M.A. Butler, D.S. Ginley, J. Electrochem. Soc. 125 (1978) 228–232.
[62] Y. Xu, M.A.A. Schoonen, Am. Mineral. 85 (2000) 543.